



Thermal Management of Nanofluid Filled Porous Cavity Utilized for Solar Heating System

Aparesh Datta¹ · Nirmalendu Biswas² · Nirmal K. Manna³ · Dipak Kumar Mandal⁴

Received: 17 February 2021 / Accepted: 5 September 2021 / Published online: 27 September 2021
© The Institution of Engineers (India) 2021

Abstract Buoyancy-driven free convection in a typical solar air heating system is investigated numerically using an indigenous code. Solar air heating (SAH) is reliable and economic for harnessing solar energy for heating/ventilation of buildings. Design, as well as application of such system/devices, needs in-depth knowledge of its transport process. To address these issues, the present study explores the fundamentals of fluid flow and heat transfer process by modeling ‘H’ shape cavity packed with saturated porous media, heated from bottom protruded body and cooled at the sides of the top protruded body, respectively. Rests of the walls are insulated. Two different working mediums (air and copper–water nanofluid) are utilized for assessing the overall thermal behavior. Evolved flow physics is analyzed and visualized for a wide range of pertinent parameters like Rayleigh number ($Ra = 10^3–10^6$), Darcy number ($Da = 10^{-7}–10^{-3}$), porosity ($\varepsilon = 0.1–1$), the concentration of nanoparticles ($\phi = 0–4\%$), and heater aspect ratio ($A = 0–2.5$) for the clear domain as well as porous domain. All the results have been visualized by streamlines, isotherms, and heat lines. The heat transfer rate is influenced significantly by the different parameters. It is observed that usage of nanofluid ensures heightened heat

transfer compared to air even in the presence of the porous medium. At higher Ra , an increasing trend of heat transfer is noted for aspect ratio from 0 to 1.0 for nanofluid (0–0.5 in case of air), beyond this heat transfer decreases, and then heat transfer increases.

Keywords Solar heating · Convection · Porous cavity · Nanofluid · Heatline · Heat transfer

Abbreviations

A	Aspect ratio of the protruded body
Da	Darcy number
h	Height of the protruded body, m
K	Permeability of the porous medium, m^2
L	Length of the cavity/length scale, m
Nu	Average Nusselt number
p	Pressure, Pa
Pr	Prandtl number
Ra	Rayleigh number
T	Temperature, K
u, v	Velocity components, m/s
U, V	Non-dimensional velocity components
w	Width of the protruded body
x, y	Cartesian coordinates, m
X, Y	Dimensionless coordinates

Greek symbols

α	Thermal diffusivity, m^2/s
β	Thermal expansion coefficient of fluid, K^{-1}
θ	Dimensionless temperature
ϕ	Nanoparticles concentrations
ε	Porosity
ν	Kinematic viscosity, m^2/s
ρ	Density, kg/m^3
σ	Electrical conductivity ($\mu \cdot Scm^{-1}$)

✉ Nirmalendu Biswas
biswas.nirmalendu@gmail.com

¹ Department of Mechanical Engineering, National Institute of Technology, Durgapur 713209, India

² Department of Power Engineering, Jadavpur University, Salt Lake, Kolkata 700106, India

³ Department of Mechanical Engineering, Jadavpur University, Kolkata 700032, India

⁴ Department of Mechanical Engineering, College of Engineering and Management, Kolaghat 721171, India

- ψ Dimensionless stream function
 Π Dimensionless heat function

Subscripts

- a Ambient
 h Heating
 f Pure fluid or base fluid (for nanofluid)
 s Solids

Introduction

Continual depletion in fossil fuel storage along with increment in environmental pollution, application of renewable energy like solar heating has gained significant attention in various domestic, agricultural as well as industrial applications. In fact, solar energy is an indispensable energy source, which can provide clean and eco-friendly power for the sustainable development of society. An effective and efficient means to feat this free and cleaner energy is to convert solar radiation into solar heating through a solar air heater (SAH). These SAH devices are simple in construction, eco-friendly, and cost-effective for converting solar radiation into thermal energy. The common applications of these devices are for room heating, ventilation, refrigeration, drying of food grains, agricultural crops, solar water desalination, solar water heater, drying of laundry, textile, and other industrial applications [1–3]. Typical SAH consist of an absorber plate and a heat exchanging medium. Heat exchanging medium may be porous structure, phase-change material, water, and others [4]. Several researchers are devoted to improving the efficacy of these heating devices.

Xiao et al. [5] have investigated (both experimentally and numerically) the invert V-shape cavity absorber fitting with fins for converting solar energy into thermal energy using heat transfer fluid (including air/ water) through a parabolic trough collector (PTC) system. They have reported the overall thermal performance of the different heat transfer fluids in the cavity under various parametric influences. Adopting the concept of a solar-assisted air heating system, Goel et al. [6] examined various parametric effects on flow dynamics and heightened thermal performance of a hemispherical cavity. Considering an inverted trapezoidal-shape cavity receiver in a solar reflector system, Reddy and Kumar [7] scrutinized the convective and radiative heat losses to maximize the solar radiation conversion into thermal energy. In another class of work, solar air-heaters are utilized for generating power through a solar chimney system. Recently, Pradhan et al. [8] thoroughly reviewed the design of a solar chimney power plant (SCPP) toward achieving enhanced performance. Considering free aspirated airflow, enhanced magnetohydrodynamic thermal

convection in a protruded heater cavity has been studied by Biswas et al. [9]. In this study, they have reported heat transfer augmentation $\sim 46\%$ with the aspirate flow.

From the knowledge of the above-mentioned background, in the present work, an attempt has been taken to explore the fundamentals of solar heating systems in a typical discrete heating and cooling system involving free convection heat transfer through a fluid-saturated porous substrate. A thorough literature review in the area of current research is carried out. A detailed account of the review on the discrete or distributed solar heating system is reported by Das and Basak [10]. Several researchers [11–14] studied the buoyancy-driven natural convection in a protruded heater/ block cavity and analyzed the heat transfer process under different parametric conditions. Such a heat transfer process is affected significantly when porous media is present. Thermal convection through porous media has been analyzed by many researchers under different thermal boundary conditions and reported that the heat transfer process decreases in the presence of porous media. Heat transfer through porous media is well documented in refs. [15, 16]. Mohebbi et al. [17] have reported about that convection is a partitioned porous cavity, applicable in typical solar power plants. Very recently, an energy-saving approach for enhancing heat transfer in a typical porous thermal cavity has been reported by Biswas et al. [18] adopting free aspiration.

Of course, the efficacy of any energy conversion system is the primary concern during the designing of a device/system pertaining to a thermal energy system. The selection of appropriate working fluid is the key parameter for improving the thermal efficiency of a system. As air is a poor conductor of heat, further improvement of thermal efficacy with air as heat transfer fluid (HTF) is limited. Thus, HTF having better thermophysical properties (like water, oil, ethylene glycol) showed interest to the researchers for enhancing thermal efficacy. Further to the above a novel coolant, ‘nanofluid/ hybrid nanofluid has been developed by the researchers with the suspension of nano-sized particles (diameter ~ 100 nm) in a carrier fluid. Due to the immersion of nanoparticles, the thermal conductivity of the carrier fluid intensified markedly. As a result, application of nanofluid/ hybrid nanofluid in different heat transfer devices/systems has been attracted. Shah and Ali [19] reported the limitation and challenges of hybrid nanofluids applications in diverse solar energy systems. Using nanofluid/ hybrid nanofluid, thermal efficacy is improved significantly even in the presence of heat transfer dampening porous medium. A detailed review of this topic can be found in [20–22].

Saleh et al. [23] numerically examined the U-shaped cavity-filled hybrid nanoparticles suspended phase-change material (PCM) immersed in water. They found that heat

transfer improvement could be more than 9% with 1% nano-capsules particles. Considering the U-shaped cavity and hot obstacle, the thermo-fluid flow behavior of Al_2O_3 –Water or TiO_2 –water nanofluid a has been numerically studied by Ma et al. [24]. They found an increasing trend of heat transfer with the increasing cavity aspect ratio. Thermal convection in an air-filled cavity with bilateral inclined solid and porous fins has been numerically investigated by Keramat et al. [25] and reported $\sim 60\%$ enhancement in heat transfer. Further works that enhanced thermal convection in cavities could be found in the literature [26–30].

The extensive review of literature illustrates the significance of thermo-fluid flow analysis in a confined space involving thermal gradient, porous structure, and nano-sized solid particles. Thus, the present study focuses to investigate thermal convection in an ‘H’ shape cavity packed with fluid-saturated porous media, heated from the bottom protruded body utilizing the solar heating system and cooled at the sides of the top protruded body, respectively, varying Rayleigh number, Darcy number, porosity, heater aspect ratio, etc. This study uses air as a working fluid initially and further, the study is extended using Cu-water nanofluid keeping in mind that the recent advancement in the development of appliances uses the engineered special fluids. Flow-through porous media is also conducted to predict the variation of thermo-physics in the cavity. Both clear and porous domains are analyzed and compared. Overall thermal performance of the thermal cavity has been compared to report better heat transfer fluid for the fixed cooling length. The dynamics of energy (heat) transportation are visualized using Bejan’s heatline [31]. The outcome from such a study can be applied to the design of solar heating/ drying/ air conditioning/ thermal storage systems.

Problem Description and Mathematical Formulation

The typical solar heating system and its simplified enlarged view of the computational geometry along with the boundary conditions are illustrated in Fig. 1. The geometry is of ‘H’ shape cavity having its side/length L . Heat is accumulated by the cavity fluid through the protruded body placed centrally at the middle of the cavity bottom wall (at temperature T_h , assuming isothermal condition); whereas the cavity hot fluid is utilized for secondary system heating by rejecting the heat (at temperature T_a) through the sides of the top protruded body. The rest of the walls are insulated. The cavity is packed with fluid ($Pr = 0.71$ and 6.93) saturated porous medium. The width of the top and bottom protrusion is taken fixed ($w = 0.2L$). Aspect ratio $A (= h/w)$ of the bottom protrusion varies from 0 and 2.5; however, in this study top protrusion aspect ratio is kept at $A = 1$.

For analyzing the evolved flow physics, flow is two-dimensional, laminar, steady, incompressible, Newtonian within the limit of Boussinesq approximation is assumed. Brinkman-Forchheimer-Darcy model (BFDM) and local thermal equilibrium model (LTE) between the porous material and fluid [15] are used for solving momentum and energy equations, considering hydrodynamically and thermally isotropic and homogeneous porous medium. The non-dimensional governing equations for mass, momentum, and energy [12, 29] can be written as:

For Air as Working Medium

$$\frac{\partial U}{\partial X} + \frac{\partial V}{\partial Y} = 0 \tag{1}$$

$$\frac{1}{\varepsilon^2} \left(U \frac{\partial U}{\partial X} + V \frac{\partial U}{\partial Y} \right) = -\frac{\partial P}{\partial X} + \frac{Pr}{\varepsilon} \left(\frac{\partial^2 U}{\partial X^2} + \frac{\partial^2 U}{\partial Y^2} \right) - \frac{Pr}{Da} U - \frac{F_c \sqrt{U^2 + V^2}}{\sqrt{Da} \varepsilon^{3/2}} U \tag{2}$$

$$\frac{1}{\varepsilon^2} \left(U \frac{\partial V}{\partial X} + V \frac{\partial V}{\partial Y} \right) = -\frac{\partial P}{\partial Y} + \frac{Pr}{\varepsilon} \left(\frac{\partial^2 V}{\partial X^2} + \frac{\partial^2 V}{\partial Y^2} \right) - \frac{Pr}{Da} V - \frac{F_c \sqrt{U^2 + V^2}}{\sqrt{Da} \varepsilon^{3/2}} V + Ra Pr \theta \tag{3}$$

$$U \frac{\partial \theta}{\partial X} + V \frac{\partial \theta}{\partial Y} = \left(\frac{\partial^2 \theta}{\partial X^2} + \frac{\partial^2 \theta}{\partial Y^2} \right) \tag{4}$$

For Nanofluid as Working Medium

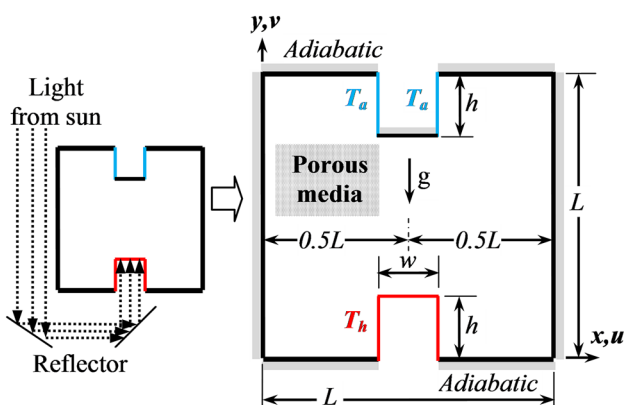


Fig. 1 Typical solar heating system and its simplified enlarged view

$$\frac{\partial U}{\partial X} + \frac{\partial V}{\partial Y} = 0 \tag{5}$$

$$\frac{1}{\varepsilon^2} \left(U \frac{\partial U}{\partial X} + V \frac{\partial U}{\partial Y} \right) = -\frac{\rho_f}{\rho} \frac{\partial P}{\partial X} + \frac{\nu \text{Pr}}{\nu_f \varepsilon} \left(\frac{\partial^2 U}{\partial X^2} + \frac{\partial^2 U}{\partial Y^2} \right) - \left(\frac{\nu \text{Pr}}{\nu_f \text{Da}} + \frac{F_c \sqrt{U^2 + V^2}}{\sqrt{\text{Da}} \varepsilon^{3/2}} \right) U \tag{6}$$

$$\frac{1}{\varepsilon^2} \left(U \frac{\partial V}{\partial X} + V \frac{\partial V}{\partial Y} \right) = -\frac{\rho_f}{\rho} \frac{\partial P}{\partial Y} + \frac{\nu \text{Pr}}{\nu_f \varepsilon} \left(\frac{\partial^2 V}{\partial X^2} + \frac{\partial^2 V}{\partial Y^2} \right) - \left(\frac{\nu \text{Pr}}{\nu_f \text{Da}} + \frac{F_c \sqrt{U^2 + V^2}}{\sqrt{\text{Da}} \varepsilon^{3/2}} \right) V + \frac{(\rho\beta)}{\rho\beta_f} \text{Ra}_m \frac{\text{Pr}}{\text{Da}} \theta \tag{7}$$

$$\left(U \frac{\partial \theta}{\partial X} + V \frac{\partial \theta}{\partial Y} \right) = \frac{\alpha}{\alpha_f} \left(\frac{\partial^2 \theta}{\partial X^2} + \frac{\partial^2 \theta}{\partial Y^2} \right) \tag{8}$$

where X and Y , U and V , P , θ are the non-dimensional coordinates, velocity components; pressure, and temperature as mentioned below.

$$(X, Y) = (x, y)/L, (U, V) = (u, v)/(\alpha_f/L), \tag{9}$$

$$P = p/\rho_f(\alpha_f/L)^2, \theta = (T - T_a)/(T_h - T_a)$$

The non-dimensional numbers: Prandtl, Rayleigh, Hartmann, and Darcy number (Pr , Ra , Ha , and Da , respectively) are defined as

$$\text{Ra} = g\beta_f(T_h - T_a)L^3/\alpha_f\nu_f, \text{Pr} = \nu_f/\alpha_f, \tag{10}$$

$$\text{Da} = K/L^2, F_c = 1.75/\sqrt{150}$$

The transportation of the heat energy from the heat source to the heat sink is illustrated using Bejan’s heatlines, which are generated after solving heat function equations [31]. Boundary conditions specified for the computation of the problem are:

- at the hot wall $U = 0, V = 0, \theta = 1$;
- at the cold wall, $U = 0, V = 0, \theta = 0$;
- at the adiabatic walls, $U = V = 0, \partial\theta/\partial Y = 0$.

To compute the characteristics of heat transfer rate from the heated surface is expressed in terms of the dimensionless form of total heat inflow q_i , total heat outflow q_o , and average Nusselt number (Nu). This quantity is calculated considering the local Nusselt number (Nu) of heating walls of the protruded body as

$$\text{Nu}_l = -\frac{\partial\theta}{\partial X} \Big|_{\text{leftwall}}, \text{Nu}_r = -\frac{\partial\theta}{\partial X} \Big|_{\text{rightwall}}, \text{ and } \text{Nu}_t = -\frac{\partial\theta}{\partial Y} \Big|_{\text{topwall}} \tag{11}$$

The heat inflow (q_i) and average Nu are calculated using

dimensionless height ($H = h/L$) and width ($W = w/L$) of the protruded body as

$$q_i = \left(\frac{k}{k_f} \right) \left[\int_0^H \text{Nu}_l dY + \int_{0.5(L-W)}^{0.5(L+W)} \text{Nu}_i dX + \int_0^H \text{Nu}_r dY \right] \tag{12}$$

The thermophysical properties of the host liquid water, denoted by subscript ‘ f ’ having $\text{Pr} = 6.93$ and Cu -nanoparticle are listed in Table 1 [20]. Cu -water nanofluid properties are calculated using the volumetric concentration of nanoparticles (ϕ) suspended in the base fluid. Following relations are utilized for obtaining the nanofluid density, specific heat, and thermal expansion coefficient:

$$\rho = (1 - \phi)\rho_f + \phi\rho_{\text{Cu}} \tag{13}$$

$$(\rho C_p) = (1 - \phi)(\rho C_p)_f + \phi(\rho C_p)_{\text{Cu}} \tag{14}$$

$$(\rho\beta) = (1 - \phi)(\rho\beta)_f + \phi(\rho\beta)_{\text{Cu}} \tag{15}$$

The effective dynamic viscosity, thermal diffusivity α , thermal conductivity (k), and effective electrical conductivity (σ) of nanofluid [20] are given by

$$\mu = \frac{\mu_f}{(1 - \phi)^{2.5}} \tag{16}$$

$$\alpha = \frac{k}{(\rho C_p)} \tag{17}$$

$$k = k_f \left[\frac{(k_s + 2k_f) - 2\phi(k_f - k_s)}{(k_s + 2k_f) + \phi(k_f - k_s)} \right] \tag{18}$$

$$\sigma = \sigma_f \left[1 + \frac{3(\sigma_s/\sigma_f - 1)\phi}{(\sigma_s/\sigma_f + 2) - (\sigma_s/\sigma_f - 1)\phi} \right] \tag{19}$$

A numerical simulation is carried out using a well-validated in-house CFD code [11, 12, 27, 30]. FVM is adopted to discretize the coupled transport equations using the SIMPLE algorithm [32] and TDMA solver. The iterative solutions of differential equations are achieved by setting the upper limiting values of mass-defect and residuals limit to $< 10^{-10}$ and 10^{-8} , respectively. Before

Table 1 The thermodynamic properties of nanoparticles and base fluid [20]

Properties	Water	Cu
$\rho(\text{kgm}^{-3})$	997.1	8933
$\mu(\text{kgm}^{-1} \text{s}^{-1})$	9.09×10^{-4}	–
$C_p(\text{J kg}^{-1} \text{K}^{-1})$	4179	385
$K(\text{W m}^{-1} \text{K}^{-1})$	0.613	401
$\beta(\text{K}^{-1})$	21×10^{-5}	1.67×10^{-5}

conducting the extensive simulation, the mesh sensitivity test (considering non-uniform grid distribution) is carried out which is not incorporated here for brevity. Finally, 190×190 grid size is selected for the present investigations.

Result and Discussion

Thermal behaviors of the studied problem of ‘H’ shape cavity heated at the bottom through protruded body utilizing solar heating approach and cooled at the top are investigated numerically. The cavity is filled with porous medium. Two different working fluids of air and Cu-water nanofluid are considered for the investigation separately. The study is conducted for wide ranges of parameters: Rayleigh numbers ($Ra = 10^3, 10^4, 10^5, 10^6$), Darcy number ($Da = 10^{-7}, 10^{-6}, 10^{-5}, 10^{-4}, 10^{-3}$), and porosity ($\varepsilon = 0.1, 0.3, 0.5, 0.6, 0.8, 1.0$) of the porous substance, heated protruded body aspect ratio ($A = 0, 0.5, 1, 1.5, 2$ and 2.5), nanofluid volume fraction, $\phi = 0$ to 4%. For the comparison, a clear domain (in absence of porous medium) is also simulated. Obtained results are presented through streamlines, isotherms, heatlines contours including average Nu, and discussed systematically for different parametric conditions below.

Assessment of Thermo-Fluid Phenomena Using Air (Pr = 0.71) as a Working Medium

Effect of Rayleigh Number

The impact of varying fluid Rayleigh number (Ra) on the thermal and fluid flow behavior is illustrated in terms of combined streamlines and isotherms (in the top row) and heatlines (in the bottom row) for the clear domain in Fig. 2a and porous domain in Fig. 2b (at $Da = 10^{-4}$, $\varepsilon = 0.6$), respectively, for $A = 1$. For the clear domain, heat energy enters into the cavity through the bottom protrusion; whereas the cavity is exchanging heat with the surroundings through the sides of the top protrusion (symmetrically located in the cavity). As a result, fluid in the cavity being hot at the lower part of the cavity flows upward and cooled after releasing heat through the heat sink (as in Fig. 2a). However, due to localized heating at the bottom and cooling at the top of the ‘H’ shape cavity, four counter-rotating symmetric circulations cells (mid horizontal plane) appear in the cavity for $Ra = 10^3$. Thus, fluid circulation forms because of temperature gradients and the weaker buoyancy effect. Corresponding isotherms are distributed from left-to-right between the bottom and top protrusion. Isotherms are noted to be curve-shaped and symmetrical

about the middle vertical axis of the cavity. It became horizontal at a distance vertically to attain the balance condition of heating and cooling.

Isotherms depicted opposite-shaped curves near the cooling zone and symmetrically about the same axis. The direction and strength of streamlines are dictated by the horizontal temperature gradient of the isotherms, thus the formation of four circulations. Bottom circulations are for heating and top are for cooling. The transport of heat energy from the heat source to the heat sink is reflected by the heatlines contour. At $Ra = 10^3$, due to conduction dominancy heat transfer, heat energy transports through a small corridor straightaway. However, as Ra increases to $Ra = 10^4$, and 10^5 , the strength and size of the lower fluid circulation cells increases as reflected by the value of the contours of streamlines. At $Ra = 10^4$, both conduction and convection mode helps to transport heat energy. The isotherms are distributed similarly in between the heat source and heat sink as observed previously, however, the isotherms curve deflects more in the heating zone and thereby formation of large circulation. Interestingly, heat energy transports from the heat source to heat sink through a long corridor; as energy circulation cells form in the lower part of the cavity closer to the side walls. However, at $Ra = 10^5$, convection mode dominates the heat transfer process. As convection increases, the maximum value stream function increases as well. The strength of the energy circulation cells rises at $Ra = 10^5$. The enhancing trend of heat transfer from the bottom heated walls of the protruded body is indicated by q_i . Cooling circulation strength decreases as the cooling area being fixed. Thermal and fluid flow behavior modify significantly with the porous medium (as in Fig. 2b). In the presence of the porous substance, resistance to fluid flow increases, resulting in a substantial decrease in maximum stream function and isotherms distributed between the heat source and heat sink. It is also pertinent to mention that two pair of circulating cells remain similar in shape, as convection force drops but the strength of the circulation increases as usual with increasing Ra . With the porous substance, energy circulation cells disappear due to poor flow as noted at Ra of 10^4 and 10^5 for the clear domain. Also, with porous medium heat transfer from the heated walls q_i (below the isotherm plots) decreases significantly due to weaker thermal convection. An increase in heat transfer like the case with clear water may be expected further at higher Ra .

The overall trends of heat transfer from the heated protruded body (q_i) with increasing Ra are indicated in Fig. 3 for both the clear and porous domains (at $Da = 10^{-4}$, $\varepsilon = 0.6$) for $A = 1$. It indicates a consistent increment in q_i for the clear domain as Ra increases beyond $Ra = 10^4$. However, with the porous domain, there is no significant increment of heat transfer compared to the clear domain.

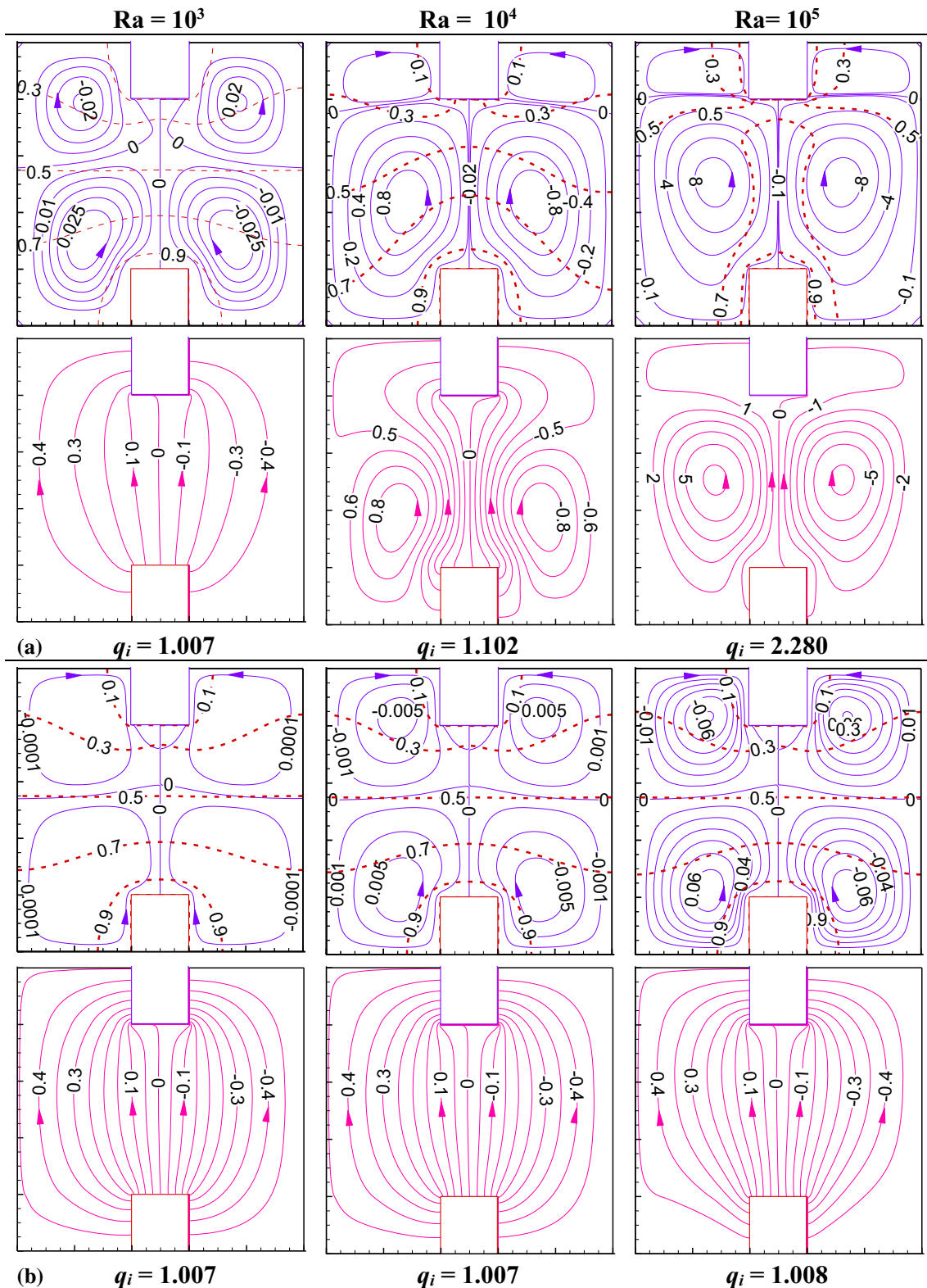


Fig. 2 Effect of Rayleigh number (Ra) on the thermal and flow fields for (a) clear (in absence of porous medium) and (b) porous domains at $Da = 10^{-4}$, $\epsilon = 0.6$, $A = 1$

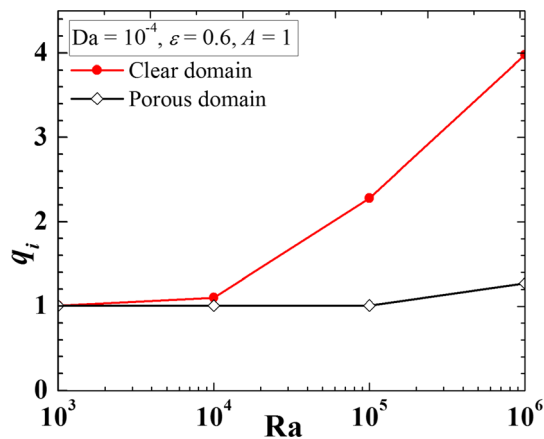


Fig. 3 Effect of Rayleigh number (Ra) on the heat transfer characteristics at $Da = 10^{-4}$, $\epsilon = 0.6$, $A = 1$

Effect of Permeability and Porosity of the Porous Medium

With the variation of Darcy number (Da) and porosity (ϵ), the influence of porous medium (resistance to fluid flow) on thermal behavior by streamlines, isotherms, and heat lines is investigated and presented in Fig. 4 at $Ra = 10^6$, $\epsilon = 0.6$, $A = 1$ and Fig. 5 at $Ra = 10^5$, $Da = 10^{-4}$, $A = 1$, respectively. No significant change in streamlines, isotherms, and heatlines is noted when Da changes from 10^{-6}

to 10^{-5} . However, major changes of bottom circulations (shape and strength) at $Da = 10^{-3}$, increasing heating corridor with passive energy circulation are noticed. This indicates a high heating value at a high Darcy number whereas it affects less at the low value of Da . Furthermore, isotherm lines are clustered with the bottom protruded body at a higher Da value. However, the effect of increasing porosity does not show major changes in the flow structure, temperature distributions, and heatlines for porosity $\epsilon = 0.3, 0.5$, and 1.0 .

Effect of Da and ϵ on heat transfer characteristics at $Ra = 10^6$, $A = 1$ is illustrated in Fig. 6, it is observed that, increase in Darcy number from 10^{-7} to 10^{-3} heat transfer rate does not change (q_i) for $Da < 10^{-5}$ for a fixed value of $\epsilon = 0.6$, $A = 1$. Of course, a significant increment in q_i is noted, which indicates improved and more heat transfer after Da of 10^{-5} . The reason for such increment is due to the decrement in resistance to fluid flow with increasing Da . As flow resistance decreases, more flow circulation establishes leading to the transportation of more amount of heat from the heat source to the heat sink depicted in streamlines, and thus, heat transfer increases. On the other hand, as porosity increases from 0.1 to 1 for a fixed value of $Da = 10^{-4}$, and $Ra = 10^6$ and $A = 1$ almost no change in heat transfer rate (q_i) is observed. A similar finding is already reported in the existing literature.

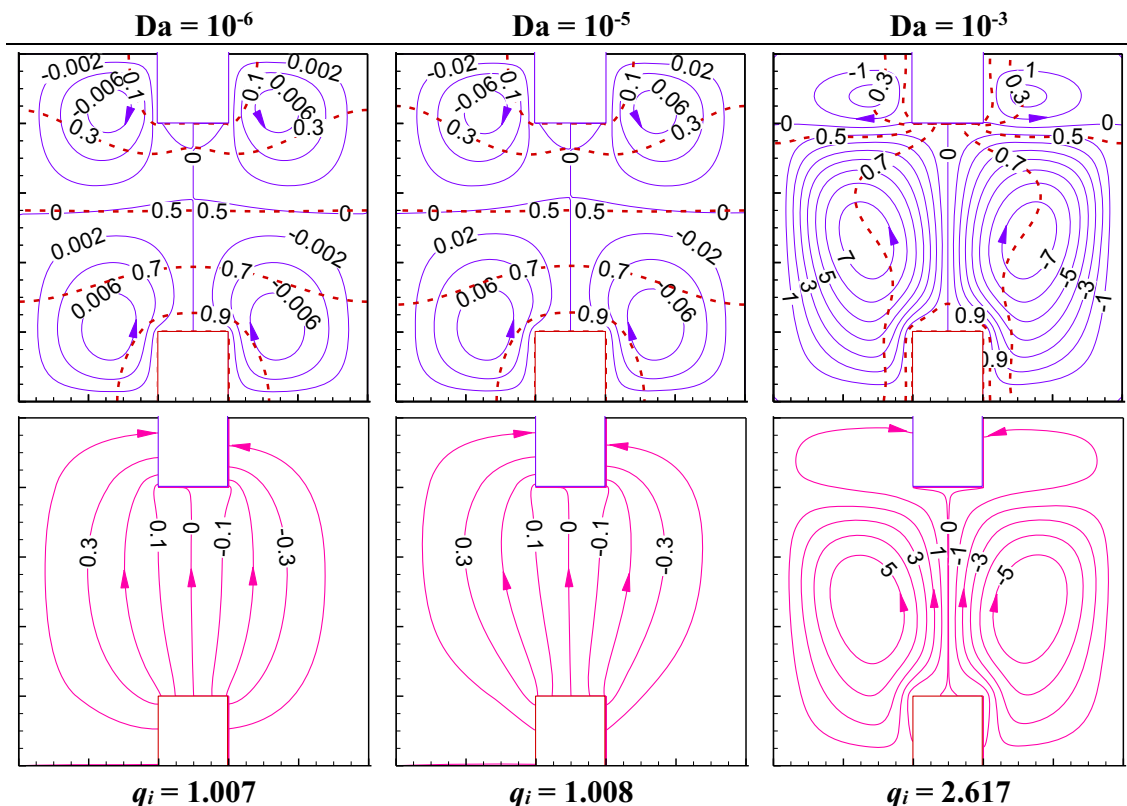


Fig. 4 Effect of Darcy number (Da) on the thermal and flow fields at $Ra = 10^6$, $\epsilon = 0.6$, $A = 1$

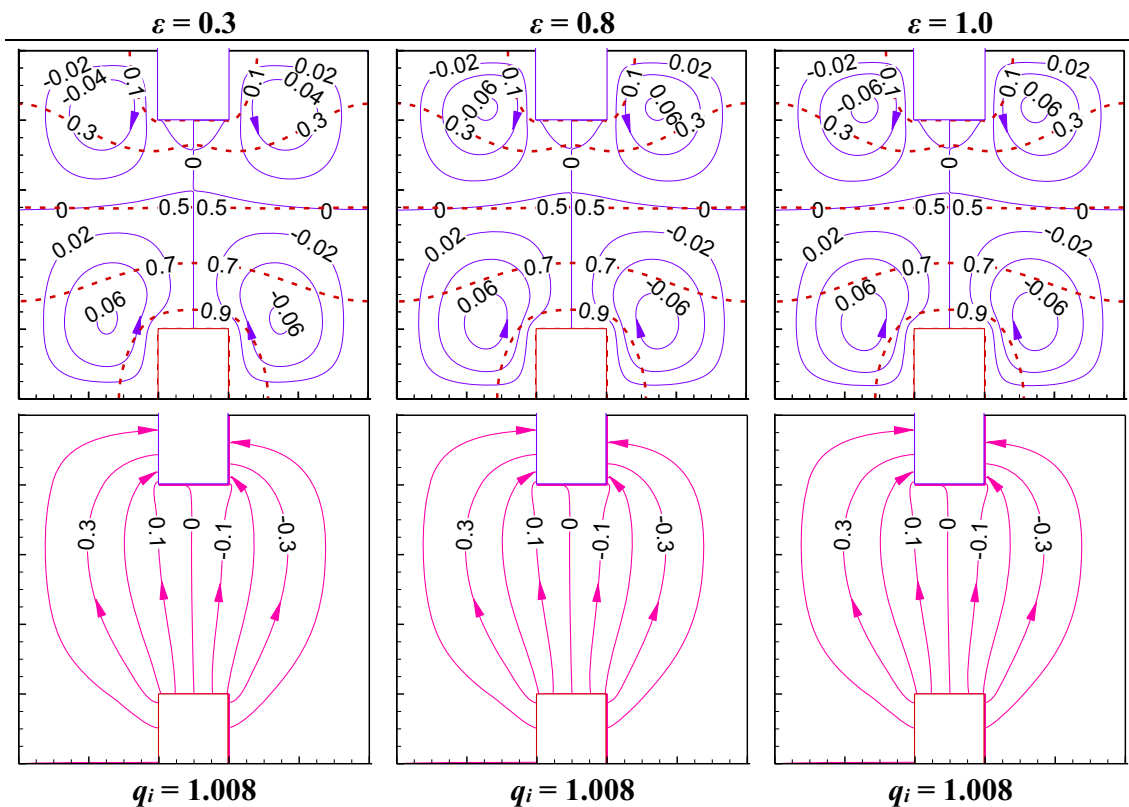


Fig. 5 Effect of porosity (ϵ) on the thermal and flow fields at $Ra = 10^5$, $Da = 10^{-4}$, $A = 1$

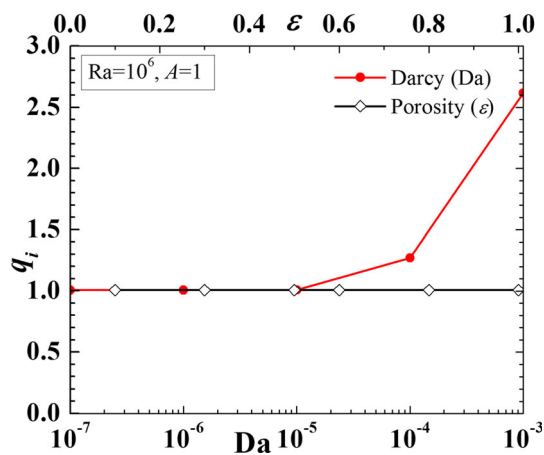


Fig. 6 Effect of Da and ϵ on the heat transfer characteristics at $Ra = 10^6$, $A = 1$

Effect of Protruded Body Aspect Ratio (A)

The influence of heat transfer surface on the flow structure and thermal behavior for different aspect ratios of the hot protruded body ($A = 0, 0.5, 2.5$) is investigated and presented in Fig. 7 for $Ra = 10^6$, $Da = 10^{-4}$, $\epsilon = 0.6$. An increase in the aspect ratio of the protruded body increases the height of the body (keeping fixed cooling length), which in turn increases the heating surface area. As a

result, more amount of heat enters into the cavity, leading to stronger fluid circulations within the cavity—as indicated by the streamlines. Interestingly, at $A = 0$ (heat-absorbing wall flushed with the bottom wall) single circulating cell (rotating in CCW direction) forms inside the cavity. Isotherms are distributed in between the top and bottom walls, its nature also supports the anticlockwise circulation inflow structure. This single-cell circulation is due to the localized heat at the bottom and discrete cooling at the top guided by the insulated sidewalls of the cavity. Heatline contours indicate that heat energy is transported from the bottom heated wall to the cold wall through the right portion of the cavity; whereas energy circulation cells form on the left portion of the cavity following the fluid circulation.

With a rise in aspect ratio to $A = 0.5$, the flow structure shows a similar pattern, but q_i is improved significantly as the heating surface area increases. However, flow structure, temperature distribution, and energy circulation patterns modify markedly when A increases to 2.5. Two pairs of symmetrical flow circulation were established about the mid-vertical plane. Lower circulation cells become larger and stronger due to higher heat energy input into the cavity fluid and higher convective flow. Corresponding isotherms are distributed in between the active walls maintain the high-temperature line adjacent to the heated body, and low-

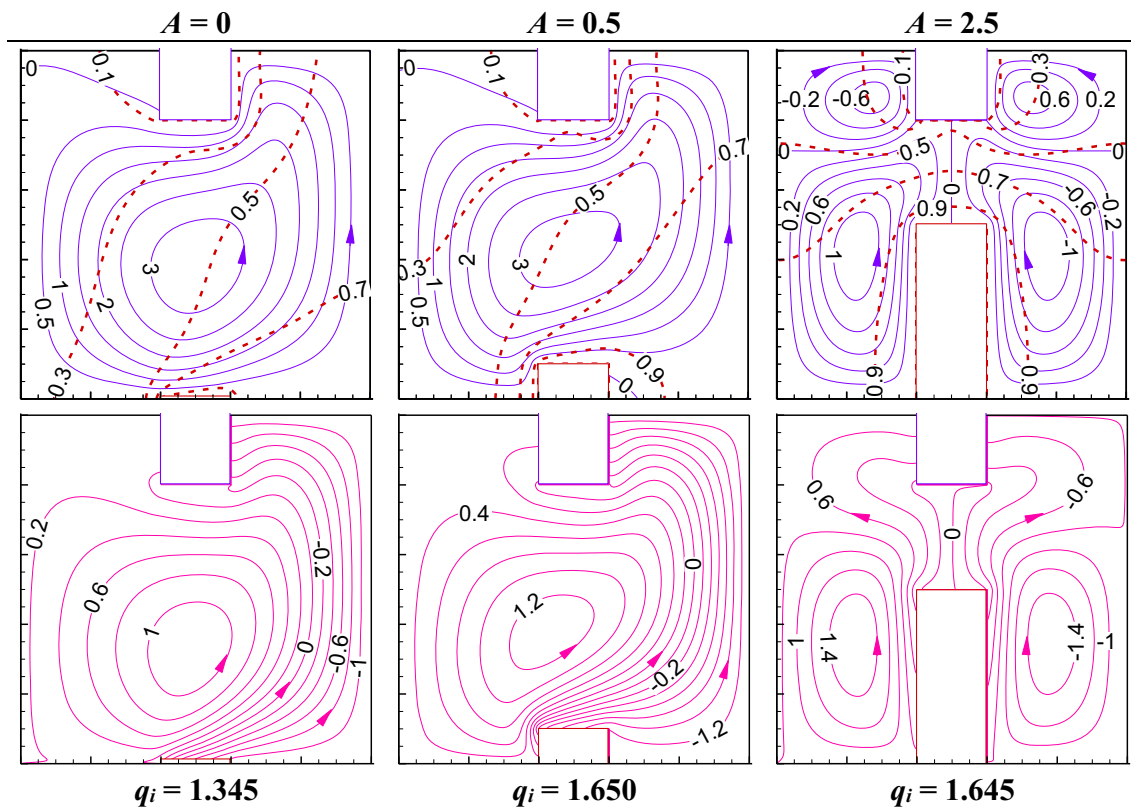


Fig. 7 Effect of protruded body aspect ratio (A) on the thermal and flow fields at $Ra = 10^6$, $Da = 10^{-4}$, $\varepsilon = 0.6$

temperature line close to the top cooling walls. Heatlines contours also show the presence of two energy circulation cells on each side of the heated protruded body. Of course, q_i increases with the increasing A . The reason for not obtaining two bottom circulations despite $A = 0.5$ is due to the small height of the protruded body which is insufficient to generate the temperature gradient in the left and right sides of the body.

Of course impact of the enhanced heating surface due to increasing protruded body height can be understood by plotting the total heat transfer (q_i) with increasing A . The trends of q_i with increasing A are presented in Fig. 8 at $Da = 10^{-4}$, $\varepsilon = 0.6$ for $Ra = 10^5$ and 10^6 . Of course, the heat transfer increases monotonously with the increasing A as the heating surface area increases at $Ra = 10^5$. However, at $Ra = 10^6$ the trend of heat transfer rate shows an unusual pattern of increment up to $A < 1$; as q_i markedly when A increases from 0 to 0.5. Beyond this q_i decreases and then heat transfer increases monotonously following a similar trend of the curve at $Ra = 10^5$. The reason for such an unusual pattern is due to the formation of a single larger circulation cell inside the cavity for $A < 1$ at a higher value

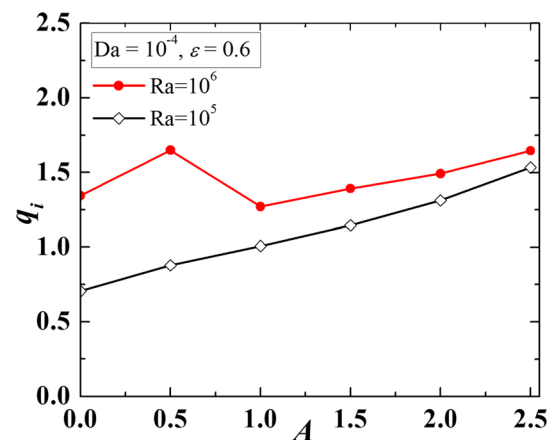


Fig. 8 Effect of protruded body aspect ratio (A) on the heat transfer characteristics q_i at $Da = 10^{-4}$, $\varepsilon = 0.6$

of $Ra = 10^6$ and after which two pairs of circulation cells forms. This influences temperature distribution inside the cavity as well as energy transportation patterns. Furthermore, there is a mutual negotiation between the increasing heating surface with the reduction in the effective working fluid volume.

Assessment of Thermo-Fluid Phenomena Using Cu-Water Nanofluid ($Pr = 6.93$)

Effect of Rayleigh Number (Ra)

The use of water being higher conductivity changes the fluid flow and heat transfer phenomena in the enclosure. The addition of a small volume of nanoparticles in water increases further the conductivity as well. Flow-through porous media alters thermo-fluid flow physics. In this section, Cu is added as a nanoparticle in water, and the investigation is made considering with or without porous media in this enclosure. In addition to the effect of nanoparticles, the effect of Ra, Da, volume fraction (ϕ), and protruded body aspect ratio (A) are analyzed for the clear domain (without porous media) and porous domain of the enclosure.

Figure 9 is shown to observe the effect of Ra (10^3 , 10^5 , 10^6) at $Da = 10^{-4}$, $\phi = 0.02$, $\varepsilon = 0.6$, $A = 1$. It is usual to note that the strength and size of the bottom streamlines increase with Ra due to the rise in buoyancy force, formation of isotherms similar to flow through the porous domain (Fig. 2b) in the case of air as a working medium. A major difference in the streamline contour with air and nanofluid is the strength of the circulation that is much more with nanofluid due to enhanced thermal convection.

Corresponding isotherm contours show marked changes as Ra increases from 10^5 to 10^6 . The heatline shows a large corridor and heat flow with two heat energy circulations at a higher Ra of 10^6 . Furthermore, the width of the heat energy transport passage increases as the magnitude of Ra increases. This implies an intensity of heat energy increases and its transport through the narrow passage.

As a results at higher Ra, two energy circulation cells forms symmetrically about the mid-vertical plane. There is no measurable change in the magnitude of heat transfer up to Ra of 10^4 (observed no change in streamlines, though it is not presented here). An increase in heat transfer is noticed with Ra for both the considered cases of the clear domain and porous domain as depicted in Fig. 10 when $Ra > 10^4$. The reason behind this may be attributed to that the heat transfer at low Ra is mostly due to conduction which is mostly convection at higher Ra (higher buoyancy force). It is also revealed that heat transfer is more in the case of the clear domain, this happens due to the reduction of flow velocity caused by the porous domain.

In comparison to the earlier consideration with air (clear as well as porous domain), it is evident that the rate of heat transfer is much larger with the nanofluid, and this is because of the presence of nanoparticles with its high thermal conductivity. Ra shows a dominant effect after 10^4 in the air like the present study with nanofluid.

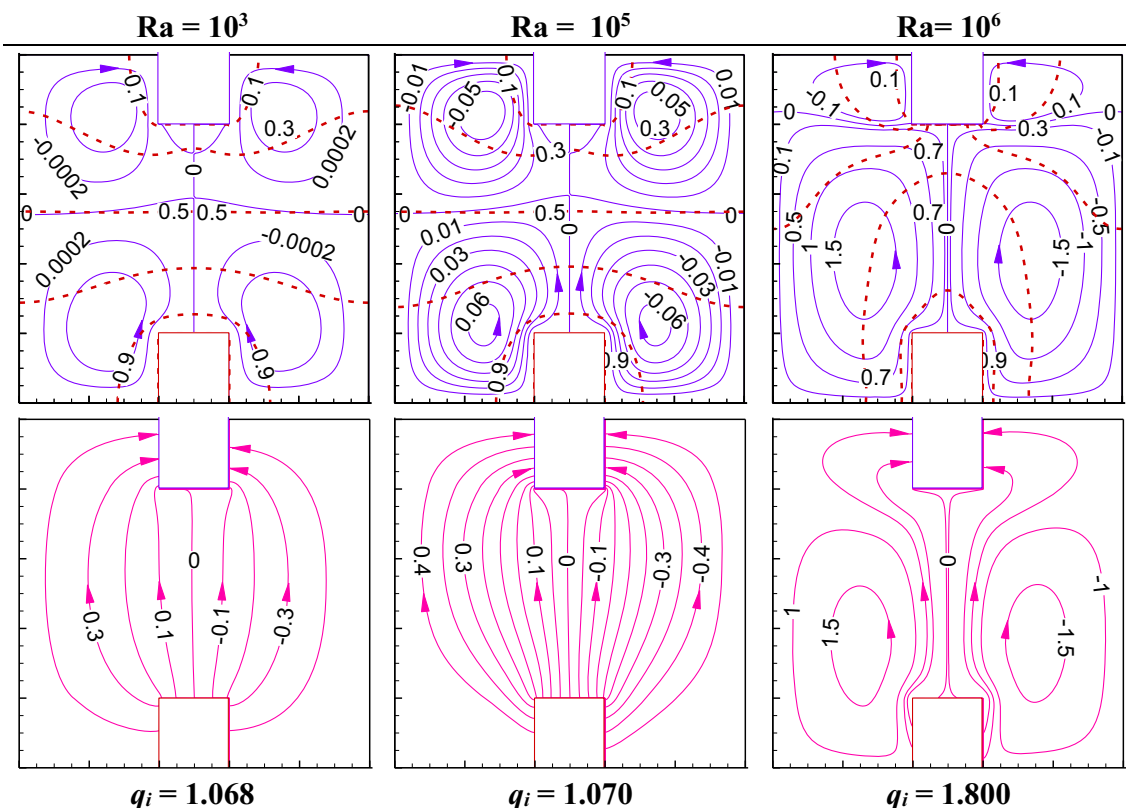


Fig. 9 Effect of Rayleigh number (Ra) on the thermal and flow fields at $Da = 10^{-4}$, $\phi = 0.02$, $\varepsilon = 0.6$, $A = 1$

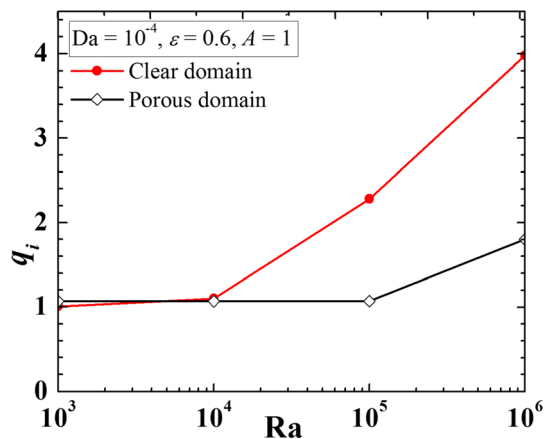


Fig. 10 Effect of Rayleigh number (Ra) on the heat transfer characteristics q_i at $Da = 10^{-4}$, $\phi = 0.02$, $\epsilon = 0.6$, $A = 1$

Effect of Darcy Number (Da)

The effect of Da at $Ra = 10^6$, $\phi = 0.02$, $\epsilon = 0.6$, $A = 1$ is illustrated in Fig. 11 by flow, temperature, and heatlines. The increase of Da from 10^{-6} to 10^{-5} does not influence the thermophysical phenomena inside the cavity too much although the flow velocity increase is caused by a poor flow. A significant change is noticed at Da of 10^{-3} , flow vortex increases its shape and strength by showing more heat transfer corridors with two passive circulations in heat

lines. This analysis is carried out with a higher fluid Rayleigh number of 10^6 . This high Ra (resulting in higher buoyancy force) does not show a major impact as the flow is restricted that reduces the convective forces. This is supported by Fig. 12 which shows no change in the heat transfer up to Da of 10^{-5} for $Ra = 10^6$, $\phi = 0.02$, $A = 1$. It is usual to obtain higher heat transfer at a higher Ra of 10^6 but after Da of 10^{-5} whereas marginal increment in q_i is noted after $Da = 10^{-4}$ with $Ra = 10^5$. This happens due to the significantly higher convective flow velocity at $Ra = 10^6$ compared to $Ra = 10^5$. At the higher Ra , fluid velocity overcomes the losses through the porous structure. The magnitude of heat transfer using nanofluid is high as compared to air but the effect of Da is noticed after 10^{-5} as compared to air as a working medium (in Fig. 6).

Effect of Nanoparticle Volume Fraction (ϕ)

Impact of addition to nanoparticle on the thermal and flow fields is shown by Fig. 13 at $Ra = 10^6$, $\epsilon = 0.6$, $A = 1$. No remarkable change in streamlines, isotherms, heat lines is observed with increases in volume fraction. This change in heat transfer is presented separately in Fig. 14 for at $Ra = 10^6$, $A = 1$, $\epsilon = 0.6$, and it shows that there is a marginal change in heat transfer, which is due to a rise in

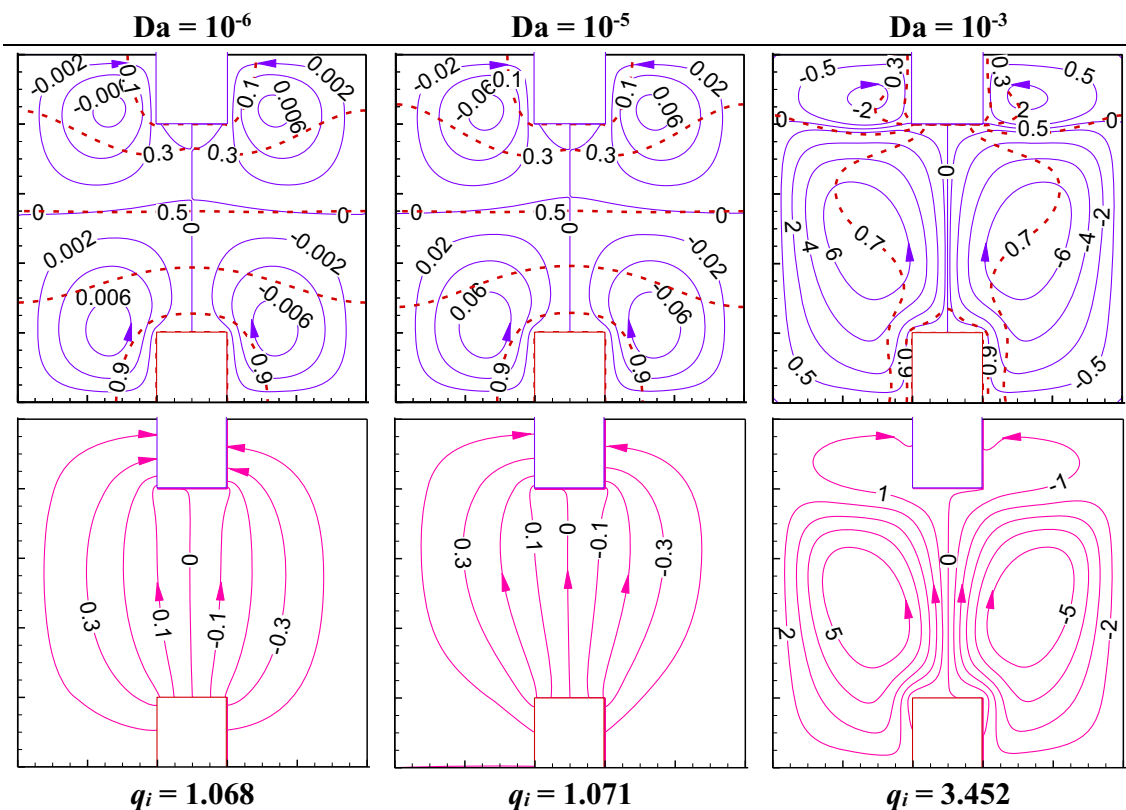


Fig. 11 Effect of Darcy number (Da) on the thermal and flow fields at $Ra = 10^6$, $\phi = 0.02$, $\epsilon = 0.6$, $A = 1$

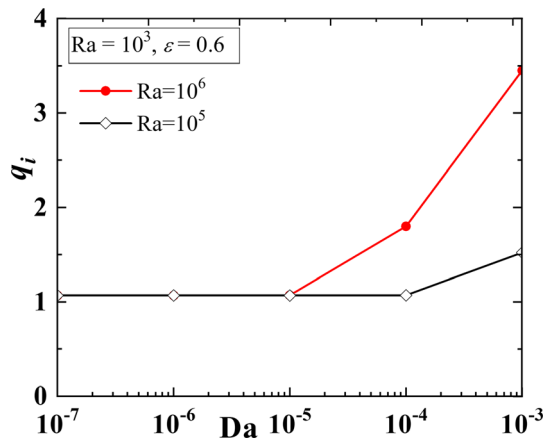


Fig. 12 Effect of Da on the heat transfer characteristics q_i at $Ra = 10^6$, $\phi = 0.02$, $A = 1$

viscosity that reduces the buoyancy force despite a high Ra of 10^6 . Further, it has been checked with a Ra of 10^5 and presented in this Fig. 14. This shows increases in heat transfer with volume fraction, this may be increased in conductivity.

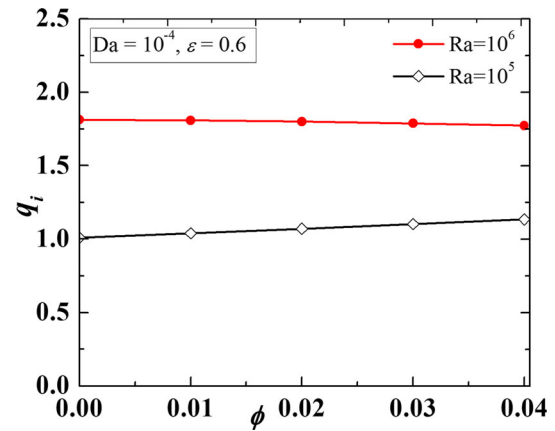


Fig. 14 Effect of nanoparticle volume fraction (ϕ) on the heat transfer characteristics q_i at $Ra = 10^6$, $A = 1$, $\epsilon = 0.6$

Effect of Protruded Body Aspect Ratio (A)

In the section, the effect of increasing protruded body aspect ratio (A) is exercised and presented in Fig. 15 for $Ra = 10^6$ and $Da = 10^{-4}$, $\phi = 0.02$, $\epsilon = 0.6$. From Fig. 15, a similar pattern is noted in the flow structure and heat transport process as noted with air as a working medium (in Fig. 7). However, an improvement in heat transfer is noted here (compared to air as a working medium). This is due to the enhanced thermal conductivity with nanofluid. To

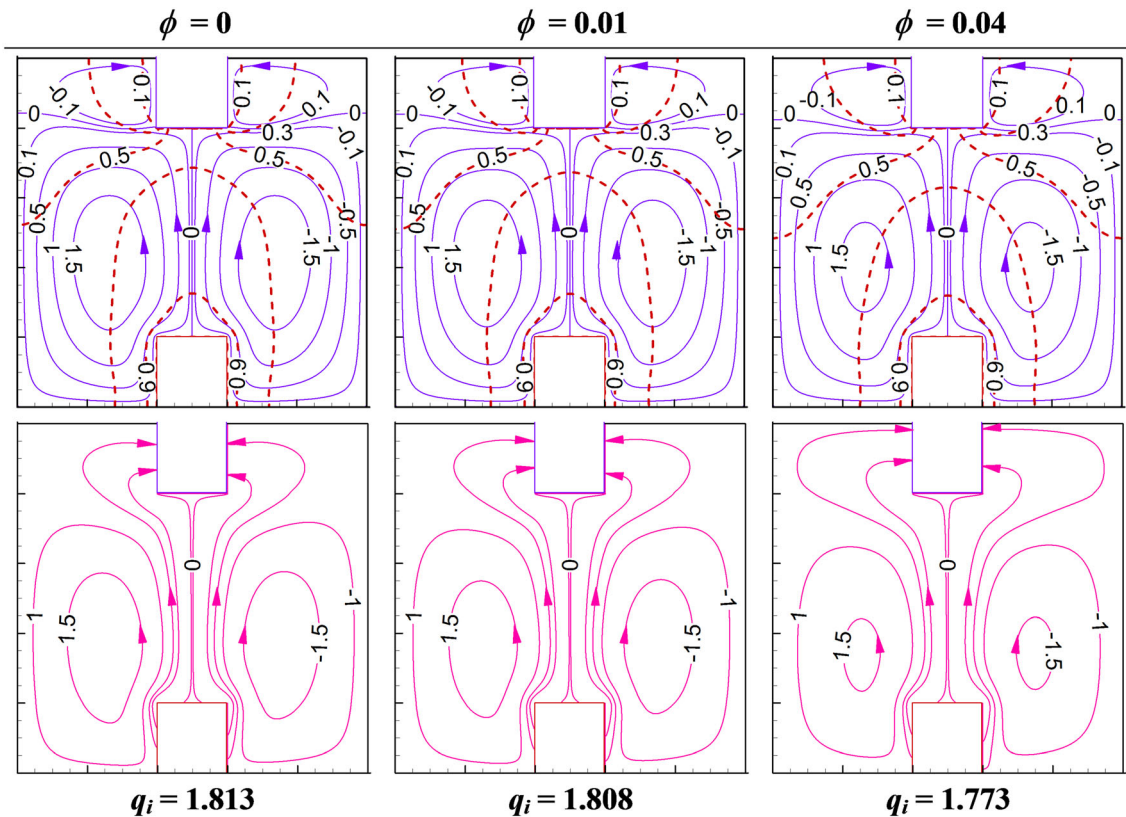


Fig. 13 Effect of nanoparticle volume fraction (ϕ) on the thermal and flow fields at $Ra = 10^6$, $\epsilon = 0.6$, $A = 1$

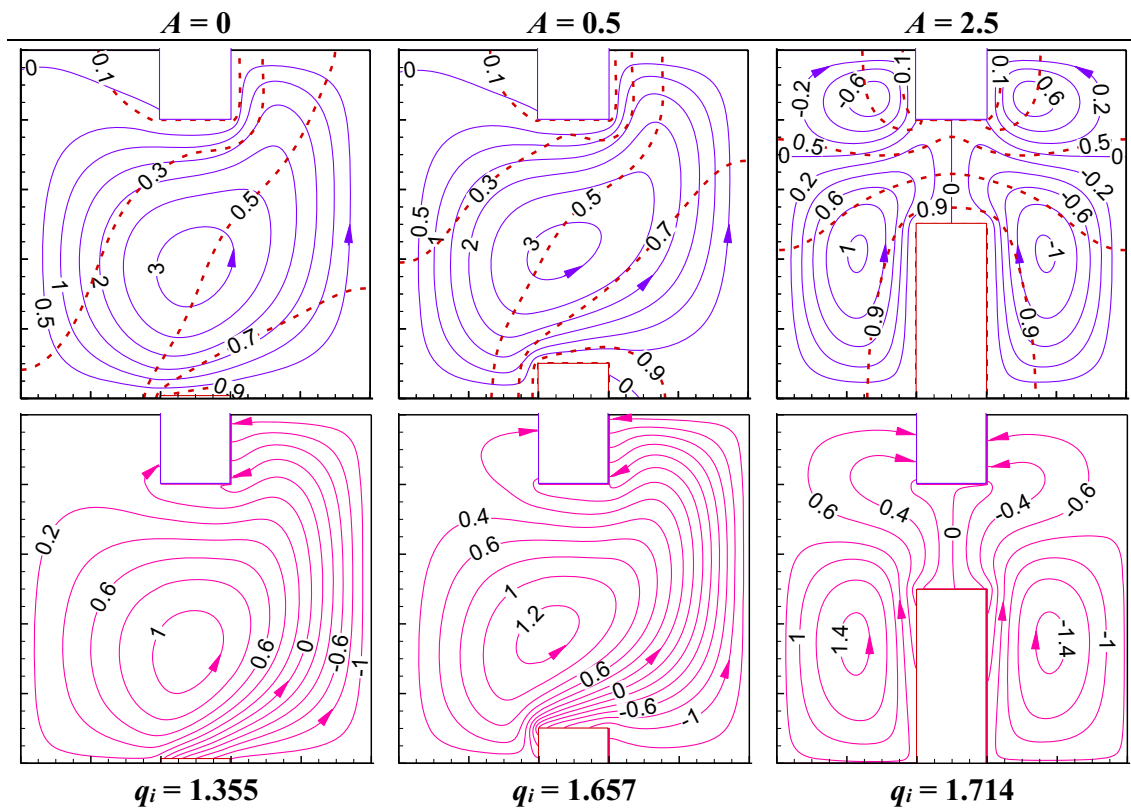


Fig. 15 Effect of protruded body aspect ratio (A) on the thermal and flow fields at $Ra = 10^6$, $Da = 10^{-4}$, $\phi = 0.02$, $\varepsilon = 0.6$

understand the global heat transfer characteristics, the effect of protruded body aspect ratio (A) on the heat transfer characteristics q_i is plotted in Fig. 16 for $Da = 10^{-4}$, $\phi = 0.02$, $\varepsilon = 0.6$. The heat transfer rate increases monotonously with the increasing aspect ratio at $Ra = 10^5$ as observed earlier with air as the working medium (in Fig. 8). At $Ra = 10^6$, the trend of heat transfer rate shows a rising tendency when A increases from 0 to 1.0 (which is from 0 to 0.5 in the case of air). Beyond this q_i decreases till $A = 1.5$ and then heat transfer increases

monotonically similar $Ra = 10^5$. The reason behind this fact is due to the change in the number of circulation from single to multiples and its orientation as the aspect ratio increases. Furthermore, as the thermal conductivity of the nanofluid is superior compared to air, magnitude of heat transfer is more with nanofluid. Thus, depending on the requirement proper selection of geometric parameters as well as flow-controlling parameters can effectively control the thermal management in a typical solar thermal system.

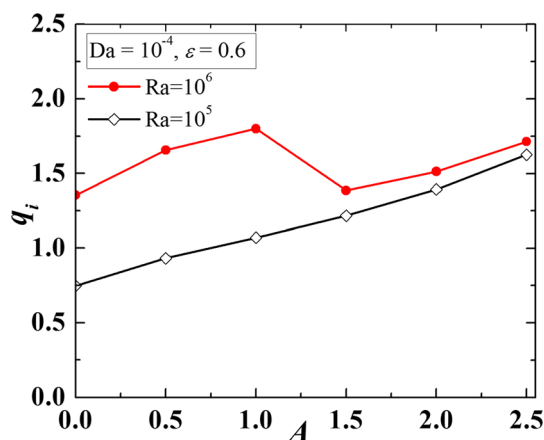


Fig. 16 Effect of protruded body aspect ratio (A) on the heat transfer characteristics q_i at $Da = 10^{-4}$, $\phi = 0.02$, $\varepsilon = 0.6$

Conclusions

Taking into consideration of solar thermal heating system, in this work, the ‘H’ shape cavity packed with fluid-saturated porous media, heated from the bottom protruded body and cooled at the sides of the top protruded body is investigated numerically under a wide range of parameters. Both air and Cu-water nanofluid are used as working fluid (separately) inside the cavity with or without porous media. The results are illustrated using streamlines, isotherms, and total heat transfer. Furthermore, the dynamics of heat energy transport are well visualized using Bejan’s heat-lines. The major observations are concluded as follows:

- The localized heating at the bottom and cooling at the top form four counter-rotating symmetric circulations

in the cavity. Heat energy is transported from the heat source to sink through a long corridor as noted by the heatlines. The width of the heat energy transport corridors is dictated by the convection strength, which is indicated by the Ra. Higher Ra ($\geq 10^4$) corresponds to more convective flow and more heat transfer.

- The use of porous domain always reduces the buoyancy force, increasing Rayleigh number ($Ra \geq 10^4$) causes more heat transfer with a clear domain compared to the porous domain for both cases of air and nanofluid. Low Rayleigh number does not affect heat transfer (for both the cases of air and nanofluid) whether the cavity with a clear domain or porous. Nanofluid increases the heat transfer as usual due to enhanced thermal conductivity of the working fluid.
- The rate of heat transfer increases with the increase in Da as the usual notion, this influences more after $Da = 10^{-5}$ both in air or nanofluid. The use of nanofluid shows superior heat transfer through the porous medium compared to air. Change in porosity has no significant impact on the heat transfer rate. With the porous domain, the effect of increasing Ra strongly depends on the Da of the porous substance.
- As the protruded body aspect ratio (A) increases, the heat transfer increases substantially. This depends on Ra. The heat transfer increases monotonously with an aspect ratio at $Ra = 10^5$ both air and nanofluid. At $Ra = 10^6$, the heat transfer rate rises for aspect ratio from 0 to 1.0 for nanofluid (0 to 0.5 in case of air), beyond this heat transfer decreases till $A = 1.5$ ($A = 1$ for air), and then heat transfer increases monotonically.
- The addition of nanoparticles does not confirm always heat transfer which depends on Ra. By the addition of nanoparticles, heat transfer increases significantly with $Ra = 10^5$, whereas the changes are marginal with $Ra = 10^6$.

Acknowledgements This article is the extended version of their presented papers during 'International Conference on Energy and Sustainable Development' held at Kolkata, India on February 14–15, 2020.

Funding There is no financial support for this work.

Declarations

Conflict of interest The authors declare that they have no conflict of interest.

References

1. S. Chamoli, R. Chauhan, N.S. Thakur, J.S. Saini, A review of the performance of double pass solar air heater. *Renew. Sustain. Energy Rev.* **16**, 481–492 (2012)
2. H. Parsa, M. Saffar-Avval, M.R. Hajmohammadi, 3D simulation and parametric optimization of a solar air heater with a novel staggered cuboid baffles. *Int. J. Mech. Sci.* **205**, 106607 (2021)
3. A.S.H. Abdallah, Passive air cooling system and solar water heater with phase change material for low energy buildings in hot arid climate. *Energy Build.* **239**, 110854 (2021)
4. S.F. Ahmed, M. Khalid, M. Vaka, R. Walvekar, A. Numan, A.K. Rasheed, N.M. Mubarak, Recent progress in solar water heaters and solar collectors: a comprehensive review. *Thermal Sci. Eng. Prog.* **25**, 100981 (2021)
5. X. Xiao, P. Zhang, D.D. Shao, M. Li, Experimental and numerical heat transfer analysis of a V-cavity absorber for linear parabolic trough solar collector. *Energy Conv. Manag.* **86**, 49–59 (2014)
6. V. Goel, R. Kumar, S. Bhattacharyya, V.V. Tyagi, A.M. Abu-sorrah, A comprehensive parametric investigation of hemispherical cavities on thermal performance and flow-dynamics in the triangular-duct solar-assisted air-heater. *Renew. Energy.* **173**, 896–912 (2021)
7. K.S. Reddy, K.R. Kumar, Estimation of convective and radiative heat losses from an inverted trapezoidal cavity receiver of solar linear Fresnel reflector system. *Int. J. Thermal Sci.* **80**, 48–57 (2014)
8. S. Pradhan, R. Chakraborty, D.K. Mandal, A. Barman, P. Bose, Design and performance analysis of solar chimney power plant (SCPP): A review. *Sus. Energy Technol. Assess.* **47**, 101411 (2021)
9. N. Biswas, N.K. Manna, A. Datta, D.K. Mandal, A.C. Benim, Role of aspiration to enhance MHD convection in protruded heater cavity. *Prog. Comput. Fluid Dyn.* **20**(6), 363–378 (2020)
10. D. Das, T. Basak, Role of distributed/discrete solar heaters during natural convection in the square and triangular cavities: CFD and headline simulations. *Sol. Energy.* **135**, 130–153 (2016)
11. N. Biswas, P.S. Mahapatra, N.K. Manna, Buoyancy-driven fluid and energy flow in protruded heater enclosure. *Meccanica* **51**, 2159–2184 (2016)
12. N. Biswas, P.S. Mahapatra, N.K. Manna, P.C. Roy, Influence of heater aspect ratio on natural convection in a rectangular enclosure. *Heat Transfer Eng.* **37**(2), 1–15 (2015)
13. M. Paroncini, F. Corvaro, Natural convection in a square enclosure with a hot source. *Int. J. Therm. Sci.* **48**(9), 1683–1695 (2009)
14. N. Biswas, S. Chatterjee, M. Das, A. Garai, P.C. Roy, A. Mukhopadhyay, (2015) Analysis of PIV measurements of natural convection in an enclosure using proper orthogonal decomposition, *ASME J. Heat Transfer* **137**, 124502–1–4.
15. D.A. Nield, A. Bejan, *Convection in Porous Media*, 4th edn. (Springer, New York, 2013)
16. A. Bejan, I. Dincer, S. Lorente, A.F. Miguel, A.H. Reis, *Porous and Complex Flow Structures in Modern Technologies* (Springer, New York, 2004)
17. R. Mohebbi, S.A.M. Mehryan, M. Izadi, O. Mahian, Natural convection of hybrid nanofluids inside a partitioned porous cavity for application in solar power plants. *J. Thermal Anal. Calorim.* **137**, 1719–1733 (2019)
18. N. Biswas, N.K. Manna, A.J. Chamkha, Energy-saving method of heat transfer enhancement during magneto-thermal convection in typical thermal cavities adopting aspiration. *SN Applied Sci.* **2**, 1911 (2020)
19. T.R. Shah, H.M. Ali, Applications of hybrid nanofluids in solar energy, practical limitations and challenges: A critical review. *Sol. Energy* **183**, 173–203 (2019)
20. K. Khanafer, K. Vafai, Applications of nanofluids in porous medium. *J. Therm. Anal. Calorim.* **135**, 1479–1492 (2019)
21. A. Kasaeian, R. Daneshzarian, O. Mahian, L. Kolsi, A.J. Chamkha, S. Wongwises, I. Pop, Nanofluid flow and heat transfer

- in porous media: a review of the latest developments. *Int. J. Heat Mass Transfer*. **107**, 778–791 (2017)
22. R.A. Mahdi, H. Mohammed, K. Munisamy, N. Saeid, Review of convection heat transfer and fluid flow in porous media with nanofluid. *Renew. Sustain. Energy. Rev.* **41**, 715–734 (2015)
 23. H. Saleh, Z. Siri, M. Ghalambaz, Natural convection from a bottom heated of an asymmetrical U-shaped enclosure with nano-encapsulated phase change material. *J. Energy Storage*. **38**, 102538 (2021)
 24. Y. Ma, R. Mohebbi, M.M. Rashidi, Z. Yang, Simulation of nanofluid natural convection in a U-shaped cavity equipped by a heating obstacle: effect of cavity's aspect ratio. *J. Taiwan Inst. Chem. Eng.* **93**, 263–276 (2018)
 25. F. Keramat, A. Azari, H. Rahideh, M. Abbasi, A CFD parametric analysis of natural convection in an H-shaped cavity with two-sided inclined porous fins. *J. Taiwan Inst. Chem. Eng.* **114**, 142–152 (2020)
 26. H. Mallick, H. Mondal, N. Biswas, N.K. Manna, Buoyancy driven flow in a parallelogrammic enclosure with an obstructive block and magnetic field. *Materials Today: Proc.* **44**(2), 3164–3171 (2021)
 27. N. Biswas, N.K. Manna, P. Datta, P.S. Mahapatra, Analysis of heat transfer and pumping power for bottom-heated porous cavity saturated with Cu-water nanofluid. *Powd. Technol.* **326**, 356–369 (2018)
 28. Q. Sun, I. Pop, Free convection in a triangle cavity filled with a porous medium saturated with nanofluids with flush mounted heater on the wall. *Int. J. Therm. Sci.* **50**, 2141–2153 (2011)
 29. N. Biswas, U.K. Sarkar, A.J. Chamkha, N.K. Manna, Magneto-hydrodynamic thermal convection of Cu–Al₂O₃/water hybrid nanofluid saturated with porous media subjected to half-sinusoidal nonuniform heating. *J. Therm. Anal. Calorim.* **143**, 1727–1753 (2021)
 30. N.K. Manna, C. Mondal, N. Biswas, U.K. Sarkar, H.F. Öztop, N.H. Abu-Hamdeh, (2021) Effect of spatially intermittently active partial magnetic fields on thermal convection in a linearly heated porous cavity filled with hybrid nanofluid, *Phys. Fluids*, **33**, 053604.
 31. S. Kimura, A. Bejan, The heatline visualization of convective heat transfer. *J. Heat Transfer*. **105**, 916–919 (1983)
 32. S.V. Patankar, *Numerical heat transfer and fluid flow*, Taylor and Francis (1980).

Publisher's Note Springer Nature remains neutral with regard to jurisdictional claims in published maps and institutional affiliations.